LAWRENCE
LIVERMORE
NATIONAL
LABORATORY

LLNL-JRNL-669426

# Stabilization of High-Compression, Indirect-Drive Inertial Confinement Fusion Implosions Using an Adiabat-Shaped Pulse

A. G. MacPhee, D. T. Casey, D. S. Clark, O. S. Jones, J. L. Milovich, J. L. Peterson, H. F. Robey, V. A. Smalyuk

April 8, 2015

Physics Of Plasmas

## Disclaimer

LLNL-JRNL-669426

# Stabilization of high-compression, indirect-drive Inertial Confinement Fusion implosions using a 4-shock adiabat-shaped drive

A.G. MacPhee, J.L. Peterson, D. T. Casey, D. S. Clark, S.W. Haan, O.S. Jones, O.L. Landen, J.L. Milovich, H.F. Robey, V. A. Smalyuk
*Lawrence Livermore National Laboratory, Livermore CA 94550, USA*

Hydrodynamic instabilities and poor fuel compression are major factors for capsule performance degradation in ignition experiments on the NIF. Using a recently developed laser drive profile with a decaying first shock to tune the ablative Richtmyer-Meshkov (ARM) instability and subsequent in-flight Rayleigh-Taylor growth, we have demonstrated reduced growth compared to the standard ignition pulse whilst maintaining conditions for a low fuel adiabat needed for increased compression. Using in-flight x-ray radiography of pre-machined modulations, the first growth measurements using this new ARM-tuned drive have demonstrated instability growth reduction of ~4x compared to the original design at a convergence ratio of ~2. Corresponding simulations give a fuel adiabat of ~1.6, similar to the original goal and consistent with ignition requirements.

Hydrodynamic instabilities have long been recognized as a major concern for inertial confinement fusion (ICF) implosions [1,2,3]. For indirect-drive implosions at the National Ignition Facility (NIF) [4] a cryogenic deuterium-tritium (DT) fuel layer is imploded by ablative acceleration of a plastic outer shell driven by x-rays generated in an enclosing hohlraum. The hohlraum is irradiated with a 1.9MJ laser pulse at up to 410TW peak power, accelerating the shell to ~400 km/s to achieve the ~1000x solid DT fuel compression required for ignition.

However, imperfections present at the outer surface of the capsule can evolve due to the ablative Richtmyer-Meshkov instability (ARM [5,6,7,8]) during shock transit through the shell and later amplified by the Rayleigh-Taylor (RT) instability [9] during the acceleration phase of the implosion. The amplified modulations can feed through the shell to the inner DT ice layer and seed a subsequent phase of RT instability growth that manifests strongly during the deceleration phase of the implosion. As a result of this instability growth, the initially spherical shell becomes distorted, leading to an asymmetric hotspot with reduced temperature, pressure, and neutron yield. In cases of extreme growth, cold ablator material can penetrate through the shell into the hotspot to mix with the DT fuel prior to peak compression, reducing temperature further and resulting in even more dramatic performance and yield degradation. The presence of ablator material mixed into the hotspot was correlated with reduced experimental yield and temperature for the high-compression layered DT implosions during the National Ignition Campaign (NIC) [10,11,12] which used the 4-shock *low-foot* drive.

During the subsequent 3-shock *high-foot* campaign [13], instability growth at the outer surface of the capsule was stabilized by putting the capsule on a higher adiabat $\alpha$. The higher $\alpha$ was achieved by launching a stronger shock during the early stage of the implosion than that used in the low-foot NIC design [14]. (The adiabat $\alpha$ is generally the ratio of the pressure to the minimum Fermi-degenerate pressure; for specific quantitative evaluation of fuel adiabat we use a definition based on mass-averaged entropy as detailed in Ref. [14]). Significant reduction in ablation front growth and hot-spot mix was observed in the high-foot campaign [15], leading to ~2x temperature increase and ~10x increased yield [16,17,18]. However, this instability growth reduction came at the expense of reduced fuel compression due to the higher DT adiabat, with $\rho R$ ~0.8 g/cm$^2$ ($\alpha$ ~2.4) for the high foot drive compared to ~1.2 g/cm$^2$ ($\alpha$ ~1.5) for the low-foot drive.

To achieve both high compression and strong ablation front stabilization for direct-drive implosions, *adiabat shaping* techniques have been developed and demonstrated at OMEGA using both decaying shock [19,20,21] and density gradient relaxation [22,21] techniques. In addition, tailored density designs were also used at NRL to stabilize growth [23], also using direct drive. In the decaying shock concept, a strong shock produced by a laser pre-pulse heats up the outer surface of the ablator putting it on a higher adiabat. During this initial drive and subsequent acceleration, the higher ablator $\alpha$ leads to higher ablation velocity that stabilizes the RT instability. When the pre-pulse switches off, the shock is no longer supported and on transit through the shell the shock decays resulting in reduced entropy transfer to the fuel, keeping the fuel on a lower adiabat required for high compression.

To understand the role of ablation-front instabilities in the high-compression implosions on NIF, *adiabat-shaped* (AS) drives were developed for indirect drive based on work by Clark *et al*. [24] for 4-shock drives (similar to the low-foot) and Peterson *et al*. [25] for 3-shock drives (similar to high-foot). In this Letter, we describe the experiments with 4-shock AS design; while the experimental results for 3-shock AS were published in Ref. [26]. In contrast to the OMEGA direct-drive cases, the indirect-drive version of adiabat-shaping uses the decaying first shock to primarily optimize the ARM oscillations [5,6] and to a much lesser extent to stabilize the RT instability growth. Increasing the laser drive early in the pulse increases the ablation pressure during shock transit through the shell, increasing the oscillation frequency and reducing the amplitude of the ARM perturbations [5]. The adiabat of the ablator starts at a similar level to that for the high-foot drive and as the first shock decays, the adiabat reduces to a level similar to that for the low-foot

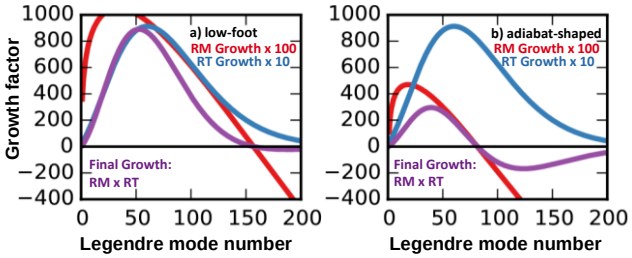


Fig. 1) Analytic estimate of combined Richtmyer-Meshkov and Rayleigh-Taylor instability growth (eqs. 22 and 16 in [27]). In the low-foot case (a), the RM node is close to mode 160, well beyond the RT growth maximum. This results in a net large and positive growth factor spectrum. For the adiabat-shaped drive (b), early time ablation velocity moves the node of the RM growth spectrum closer to the maximum of the RT growth spectrum, resulting in significantly reduced net RM-RT growth.

drive. For indirect-drive NIF implosions, modes near the peak of the ablative RT growth spectrum undergo ~1 ARM oscillation prior to RT amplification. The net effect is that the low mode numbers experience positive growth and high mode numbers experience negative growth, and the mode number of the node undergoing zero growth scales inversely with the strength of the first shock [27]. Such phase reversal has been observed previously for direct drive [28,29] but not for indirect drive [30,31] until reported recently by Peterson *et al.* [32]. Using such phase reversal it is possible to optimally tune the ARM seed to the RT instability by placing the zero growth node near the peak of the RT growth, reducing the overall effect of instability growth comprising ARM oscillations and the RT instability as shown schematically in Fig. 1. (For detailed fuel-ablator and ablation front growth factor spectra, including those for the high-foot case see Ref. [27]).

Fig. 2a shows the laser pulse shapes for the low-foot, high-foot, and new 4-shock adiabat-shaped drive. The 4-shock design optimizes the low-foot ARM phase by increasing the laser *picket* (the pulse that launches the first shock), whilst maintaining the laser *trough* at similar intensity (the low intensity region between the picket and the main drive). The pulse shape was determined [24] through a series of detailed radiation-hydrodynamic simulations using the HYDRA code [33]. Subsequent hohlraum simulations, also performed with HYDRA, were then used to determine the laser pulse necessary to achieve these optimal implosion characteristics [34]. The picket energies and average trough powers are 15kJ, 38kJ, and 23kJ and 1.4 TW, 4 TW, and 1.4 TW respectively. Both higher power and longer duration pickets increase the initial $T_r$ and hence the first shock strength. This can be seen in Fig. 2b, simulated pressure behind the 1st shock on transit from the ablation front to the fuel is plotted verses the locus of this point in the radial direction. Measurements of the first shock velocity using VISAR (Velocity Interferometry System for Any Reflector [35]) confirmed the behavior shown in Fig. 2b. using the drives in Fig. 2a [36].

As intended, the high-foot drive exhibits increased adiabat at both the ablator and the fuel compared to the low-foot drive for which pressure remains essentially constant throughout. The first shock launched by the adiabat-shaped drive into the ablator has initial strength similar to high-foot. However, with the trough lower by a factor of ~4 the unsupported shock decelerates on transit through the ablator resulting in reduced entropy deposits in the fuel, at a level similar to that for the low-foot drive and provides the appropriate starting conditions for a high convergence low mix implosion.

Following the previous growth study for the low-foot and high-foot drives [15], x-ray radiographic measurements of the optical depth amplitude growth of pre-imposed modulations in the shell of an indirect-drive ICF capsule using the adiabat-shaped drive were made at Legendre mode numbers $\ell$ = 60 and 90 (where $\ell = 2\pi R_0/\lambda_0$, $R_0$ is the capsule radius at the modulation nodes and $\lambda_0$ is the initial modulation wavelength) up to a convergence ratio $R_0/R \approx 2$. The experimental platform is described in [37] and illustrated in Fig. 3. The targets were silicon-doped plastic capsules with outer radii 1120 μm and shell thickness 206 μm. These shells were 14 μm thicker than equivalent cryogenic layered DT capsules, with extra CH ablator material added to replace the DT fuel of an ignition target. (For a detailed discussion on target surrogacy, see [38]). Sinusoidal modulations with $\lambda$ = 120 μm and $\lambda$=80 μm, and peak-to-valley amplitude 0.5 μm and 0.6 μm respectively were machined into the outer surface of the capsule on either side of the line of sight of a 1D space resolving x-ray framing camera, giving simultaneous measurement of optical depth modulation at Legendre modes 60 and 90 on the same shot. The gold re-entrant cone provides an unobstructed path for the backlighter to the ripples along the camera line of sight and is sealed to the hohlraum wall to maintain 0.96 mg/cm$^3$ $^4$He in the hohlraum, while maintaining the capsule interior at chamber vacuum via the cone. The framing camera was timed to gate four ~80 ps radiographs at ~400 ps intervals projected by the ~3 ns duration ~5.4 keV Vanadium Ly-α/He-α backlighter. The resulting images span the acceleration phase of the capsule up to a convergence ratio of ~2.

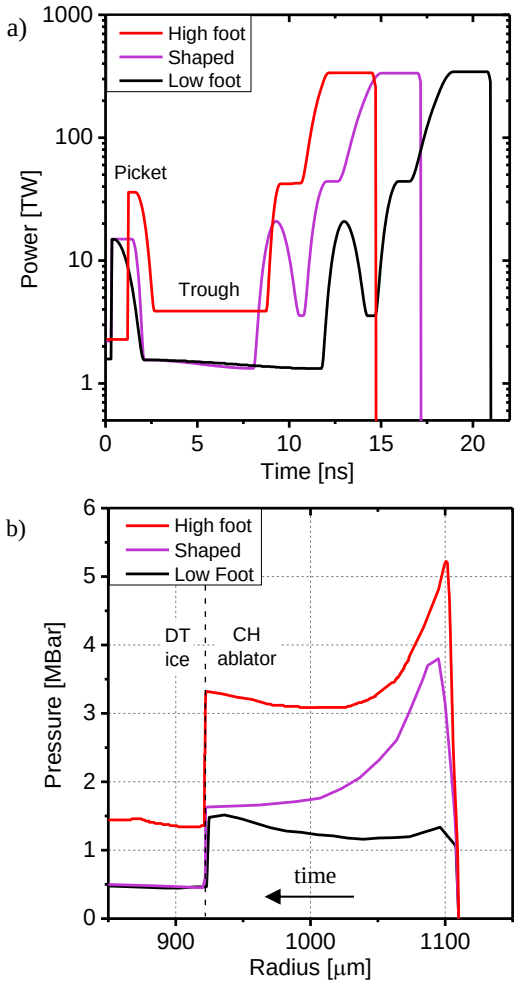


Fig. 2: a) laser pulse shapes and b) pressures behind the leading shock on transit from the ablation front to the fuel.

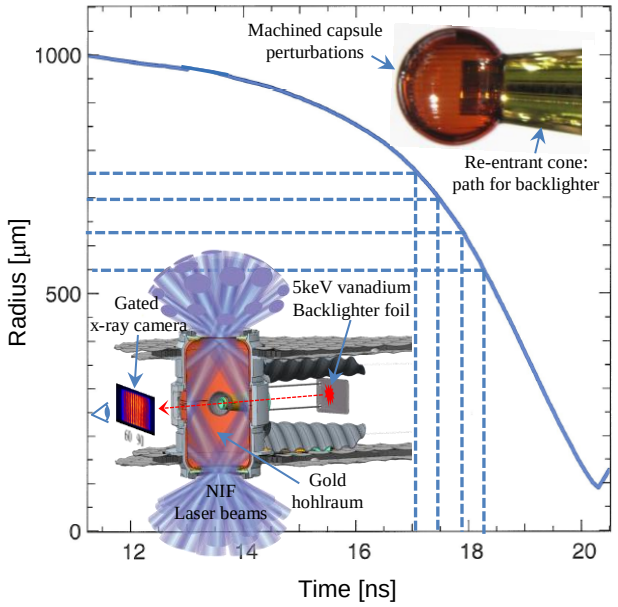


Fig. 3) Simulated capsule trajectory with four x-ray camera gate times. Inserts: Cutaway view of hohlraum with re-entrant cone and Vanadium backlighter foil; photo of capsule with gold cone and machined ripples.

Radiographs of the modulations at modes 60 and 90 for the three pulse shapes at capsule radius $r$ ~550 μm and the corresponding optical depth amplitude plots are shown in Fig. 4. Here $\Delta OD = -\Delta\ln(I/I_0) = \Delta\int \kappa\,\rho dR$ where the opacity $\kappa$ is for the backlighter x-ray energy of 5.4 keV and $\rho dR$ is the projected areal density at each point across the ripple profile. $I$ and $I_0$ are the transmitted and incident backlighter intensities, respectively. At convergence ratio ~2, the optical depth modulation amplitude at mode 60 is reduced by a factor of ~2 for both the high-foot and the adiabat-shaped drives as compared to low-foot drive. The significant optical depth modulation amplitude observed for the low-foot drive at mode 90 is essentially eliminated for the high-foot drive and is reduced by a factor of ~3 and inverted in phase for the adiabat-shaped drive. Reduced growth at mode 60 in the vicinity of the dispersion curve peak compared to the low-foot measurements quantifies the magnitude of the total instability growth reduction, while phase inversion at mode 90 in the vicinity of peak negative growth confirms that this reduction was achieved by optimizing the ARM growth phase, through a shift of the zero crossing to lower mode number as predicted by modeling.

Figure 5 combines the OD modulation data vs radius for the three pulse shapes at the four gate times on the detector, corrected for the modulation transfer function of the imaging slit. The measured OD modulation amplitude indicated for the high-foot drive at mode 90, at just above the measurement noise level, represents an upper limit on the modulation amplitude for all four radii. Both the high-foot and adiabat-shaped drives achieved a similar level of growth stabilization compared to the low-foot drive and agree well with the post-shot HYDRA simulations indicated by the shaded regions in the figure (for a discussion of simulation uncertainties, see [32] from which the low-foot; high-foot simulations are reproduced). These observations are consistent with a shift in the total-growth spectrum zero-crossing to lower mode number for both the high-foot and adiabat-shaped drives as predicted by both theory and simulations, where the increased ablation pressure during shock transit through the shell increases the oscillation frequency and reduces the amplitude of the ARM instability perturbations.

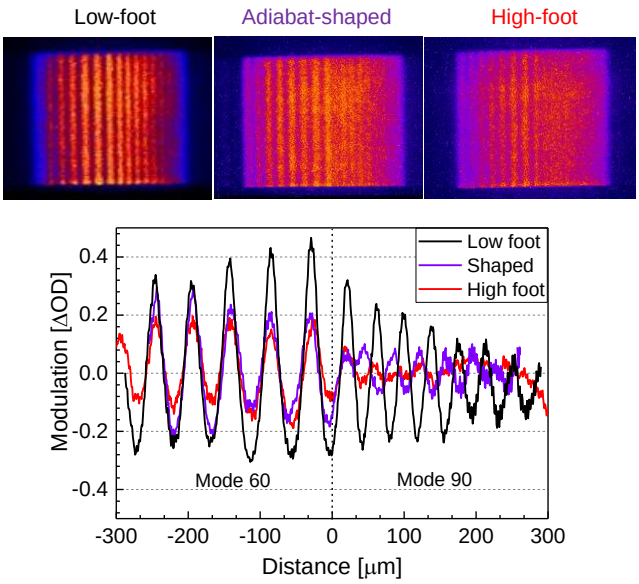


Fig. 4) Gated x-ray images (top) and optical depth profiles (bottom) for the three pulse shapes (r ~550μm). Low-foot, high-foot data reproduced from [15]. Mode 90 for the adiabat-shaped drive had inverted phase compared to the low-foot drive while mode 60 had the same phase for all drives.

By linear interpolation between the OD amplitude at modes 60 and 90, the ARM node for the adiabat-shaped drive is inferred to be at mode ~80. By contrast, the high-foot and low-foot drive ARM nodes are measured at mode 120 and just beyond mode 160, respectively [32]. The locations of the zero-growth nodes can be understood in terms of ARM instability [5] as applied to indirect-drive implosions [27]. The first shock's vorticity deposition upon interacting with an initially rippled surface at mode $l = kR$ causes an ablation surface oscillation with decaying amplitude ~$\sin(kV_a t\sqrt{3})/\sqrt{kV_a t}$, where $R$ is the ablation front radius, $k$ is the wavenumber of the oscillation, $V_a$ is the characteristic ablation velocity and $\sqrt{3}$ accounts for the 3x compression by the first shock [39]. From this vorticity term alone, one would expect the mode number for zero growth $l_0$ to scale as $(V_a t_l)^{-1}$. Putting in numbers for the low-foot case, R = 1100 μm, $V_a = 1$ μm/ns [27], and $t_l$ the time difference between 1st and 2nd shock launch, approximately equal to the picket + trough duration, = 12 ns, the first node $l_0 = (\pi/\sqrt{3})(R/V_a t) \approx 170$, close to what is found experimentally. In detailed analytic derivations and simulations of NIF ICF ARM dynamics [27], there is an additional significant dynamic overpressure term sensitive to a mode dependent blow-off velocity which leads to $l_0$ scaling more precisely as $l_0 \sim V_a^{-1.49} t_l^{-0.94}$. Per same reference [27], the average ablation rate in picket and trough as only the picket energy is varied scales as ~ $T_r^{2.2}$, where $T_r$ here is defined as the peak picket temperature. Hence for the measured $T_r$ = 119 vs 88 eV for adiabat-shaped vs low-foot drives [36] (consistent with 3x initial pressure ratio on Fig. 2b since $P \sim T_r^{3.2}$ in the foot of pulse [36]), the average $V_a$ ratio = 2x. So $\frac{l_{0AS}}{l_{0LF}} = 2^{-1.49}\left(\frac{8}{12}\right)^{-0.94} \simeq 0.5$, which agrees with the hydro-growth measurements showing $l_{0AS} \sim 80$ and $l_{0LF} \geq 160$. For

the high-foot case, the increase in $V_a$ is largely offset by the reduced $t_l$ which puts the zero crossing at higher mode number ($l_{0HF}$~120, see [32]). It is interesting to note that even though $l_{0HF}$ is larger than $l_{0AS}$ (and thus less optimal for ARM growth) the total growth observed at mode 60 is similar. Lower RT growth for the high-foot drive, consistent with the shallower optical depth growth trajectory in Fig. 5, could account for this.

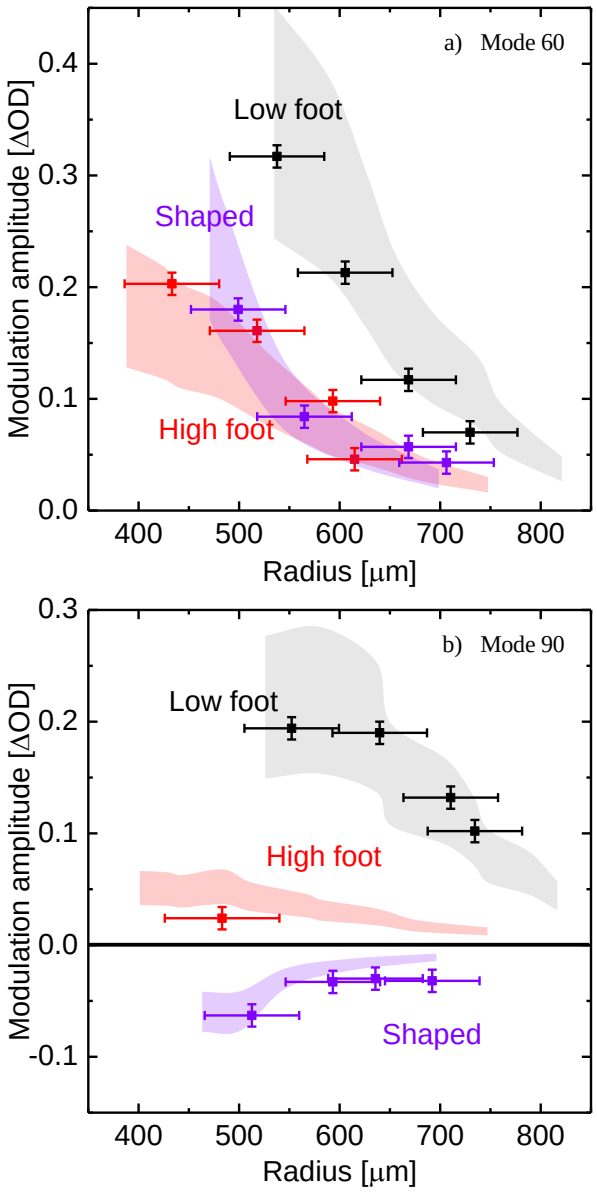


Fig. 5) Optical depth modulation vs radius at a) mode 60 and b) mode 90 for the three pulse shapes. Low-foot and high-foot data and simulations are reproduced from [15,32] for direct comparison with the adiabat-shaped data.

In summary, we have demonstrated an indirect-drive ICF platform with a stabilized ablation front that also maintains a low fuel adiabat at the inside surface of the ablator leading to increased fuel compression and hence the potential for increased temperature and yield for DT layered implosions. Hydro-growth radiography experiments were performed for the three pulse shapes measuring instability growth in the vicinity of the peak and the first ARM node. Using a pulse shape with similar picket intensity to the high-foot drive and similar trough intensity to the low-foot drive, stabilization similar to the high-foot drive was achieved. Combining these results with the related measurements from [36], which quantified the fuel adiabat for these pulses, presents a very promising path forward for achieving implosions with both low levels of degradation from mix and the potential for high fuel compression. Experiments are currently underway to test the performance of DT layered implosions employing these new stable, high-compression pulses.

The authors would like to thank R. Betti, V. N. Goncharov, J. Lindl, and D. Shvarts for useful discussions. This work was performed under the auspices of the U.S. Department of Energy by Lawrence Livermore National Laboratory under Contract DE-AC52-07NA27344.

**References**

[1] J. H. Nuckolls, L. Wood, A. Thiessen, G. Zimmerman, Nature **239**, 139 (1972)
[2] J. D. Lindl, P Amendt, R. L. Berger, S. Gail Glendinning, Siegfried H. Glenzer, Steven W. Haan, Robert L. Kauffman, Otto L. Landen and Laurence J. Suter, Phys. Plasmas **11**, 339 (2004)
[3] J. H. Nuckolls, Journal of Physics: Conference Series **244** 012007 (2010)
[4] E. I. Moses, R. N. Boyd, B. A. Remington, C. J. Keane, and R. Al-Ayat,, Phys. Plasmas **16**, 041006 (2009); G. H. Miller, E. I. Moses, C. R. Wuest, Opt. Eng. 443, 2841 (2004)
[5] V. N. Goncharov, Phys. Rev. Lett. **82**, 2091 (1999)
[6] Y. Aglitskiy, A. L. Velikovich, M. Karasik, V. Serlin, C. J. Pawley, A. J. Schmitt, S. P. Obenschain, A. N. Mostovych, J. H. Gardner and N. Metzler, PRL **87**, 265001 (2001)
[7] E. E. Meshkov, Izv. Acad. Sci. USSR Fluid Dynamics **4**, 101 (1969); R. D. Richtmyer, Commun. Pure Appl. Math. **13**, 297 (1960)
[8] T. Endo, K. Shigemori, H. Azechi, A. Nishiguchi, K. Mima, M. Sato, M. Nakai, S. Nakaji, N. Miyanaga, S. Matsuoka, A. Ando, K. A. Tanaka, and S. Nakai, Phys. Rev. Lett **18**, 3608 (1995)
[9] Lord Rayleigh, Proc. London Math. Soc. **s1-14**, 170 (1882); G. I. Taylor, Proc. R. Soc. London, Ser. A 201, 192 (1950)
[10] M. J. Edwards, J. D. Lindl, B. K. Spears, S. V. Weber , L. J. Atherton , D. L. Bleuel , D. K. Bradley , D. A. Callahan , C. J. Cerjan , D. Clark , G. W. Collins , J. E. Fair , R. J. Fortner , S. H. Glenzer , S. W. Haan , B. A. Hammel , A. V. Hamza , S. P. Hatchett , N. Izumi , B. Jacoby , O. S. Jones , J. A. Koch , B. J. Kozioziemski , O. L. Landen , R. Lerche , B. J. MacGowan , A. J. MacKinnon , E. R. Mapoles , M. M. Marinak , M. Moran , E. I. Moses , D. H. Munro , D. H. Schneider , S. M. Sepke , D. A. Shaughnessy , P. T. Springer , R. Tommasini , L. Bernstein , W. Stoeffl , R. Betti , T. R. Boehly , T. C. Sangster , V. Y. Glebov , P. W. McKenty , S. P. Regan , D. H. Edgell , J. P. Knauer , C. Stoeckl , D. R. Harding , S. Batha , G. Grim , H. W. Herrmann , G. Kyrala , M. Wilke , D. C. Wilson , J. Frenje , R. Petrasso , K. Moreno , H. Huang , K. C. Chen , E. Giraldez , J. D. Kilkenny , M. Mauldin , N. Hein , M. Hoppe , A. Nikroo , and R. J. Leeper, Phys. Plasmas **18**, 051003 (2011)
[11] S. P. Regan, R. Epstein, B. A. Hammel, L. J. Suter, H. A. Scott, M. A. Barrios, D. K. Bradley, D. A. Callahan, C. Cerjan, G. W. Collins, S. N. Dixit, T. Döppner, M. J. Edwards, D. R. Farley,

K. B. Fournier, S. Glenn, S. H. Glenzer, I. E. Golovkin, S. W. Haan, A. Hamza, D. G. Hicks, N. Izumi, O. S. Jones, J. D. Kilkenny, J. L. Kline, G. A. Kyrala, O. L. Landen, T. Ma, J. J. MacFarlane, A. J. MacKinnon, R. C. Mancini, R. L. McCrory, N. B. Meezan, D. D. Meyerhofer, A. Nikroo, H.-S. Park, J. Ralph, B. A. Remington, T. C. Sangster, V. A. Smalyuk, P. T. Springer and R. P. J. Town, Phys. Rev. Lett. **111**, 045001 (2013)
[12] T. Ma, P. K. Patel, N. Izumi, P. T. Springer, M. H. Key, L. J. Atherton, L. R. Benedetti, D. K. Bradley, D. A. Callahan, P. M. Celliers, C. J. Cerjan, D. S. Clark, E. L. Dewald, S. N. Dixit, T. Döppner, D. H. Edgell, R. Epstein, S. Glenn, G. Grim, S. W. Haan, B. A. Hammel, D. Hicks, W. W. Hsing, O. S. Jones, S. F. Khan, J. D. Kilkenny, J. L. Kline, G. A. Kyrala, O. L. Landen, S. Le Pape, B. J. MacGowan, A. J. Mackinnon, A. G. MacPhee, N. B. Meezan, J. D. Moody, A. Pak, T. Parham, H.-S. Park, J. E. Ralph, S. P. Regan, B. A. Remington, H. F. Robey, J. S. Ross, B. K. Spears, V. Smalyuk, L. J. Suter, R. Tommasini, R. P. Town, S. V. Weber, J. D. Lindl, M. J. Edwards, S. H. Glenzer, and E. I. Moses, Phys. Rev. Lett. **111**, 085004 (2013)
[13] T. R. Dittrich, O. A. Hurricane, D. A. Callahan, , E. L. Dewald, T., Doeppner, D. E. Hinkel, L. F. Berzak Hopkins, S. LePape, T. Ma, J. L. Milovich, J. C. Moreno, P. K. Patel, H.-S. Park, B. A. Remington and J. D. Salmonson, Phys. Rev. Lett. **112**, 055002 (2014)
[14] S. W. Haan, J. D. Lindl, D. A. Callahan, D. S. Clark, J. D. Salmonson, B. A. Hammel, L. J. Atherton, R. C. Cook, M. J. Edwards, S. Glenzer, A. V. Hamza, S. P. Hatchett, M. C. Herrmann, D. E. Hinkel, D. D. Ho, H. Huang, O. S. Jones, J. Kline, G. Kyrala, O. L. Landen, B. J. MacGowan, M. M. Marinak, D. D. Meyerhofer, J. L. Milovich, K. A. Moreno, E. I. Moses, D. H. Munro, A. Nikroo, R. E. Olson, K. Peterson, S. M. Pollaine, J. E. Ralph, H. F. Robey, B. K. Spears, P. T. Springer, L. J. Suter, C. A. Thomas, R. P. Town, R. Vesey, S. V. Weber, H. L. Wilkens and D. C Wilson, Phys. Plasmas **18**, 051001 (2011)
[15] D. T. Casey, V. A. Smalyuk, K. S. Raman, J. L. Peterson, L. Berzak Hopkins, D. A. Callahan, D. S. Clark, E. L. Dewald, T. R. Dittrich, S. W. Haan, D. E. Hinkel, D. Hoover, O. A. Hurricane, J. J. Kroll, O. L. Landen, A. S. Moore, A. Nikroo, H.-S. Park, B. A. Remington, H. F. Robey, J. R. Rygg, J. D. Salmonson, R. Tommasini, and K. Widmann, Phys. Rev. E **90**, 011102(R) (2014)
[16] O. A. Hurricane, D. A. Callahan, D. T. Casey, P. M. Celliers, C. Cerjan, E. L. Dewald, T. R. Dittrich, T. Döppner, D. E. Hinkel, L. F. Berzak Hopkins, J. L. Kline, S. Le Pape, T. Ma, A. G. MacPhee, J. L. Milovich, A. Pak, H.-S. Park, P. K. Patel, B. A. Remington, J. D. Salmonson, P. T. Springer & R. Tommasini, Nature **506**, 343 (2014)
[17] R. Tommasini, Bull. Am. Phys. Soc. 59, 237 (2014)
[18] H-S. Park, O. A. Hurricane, D. A. Callahan D. T. Casey, E. L. Dewald, T. R. Dittrich, T. Doeppner, D. E. Hinkel, L. F. Berzak Hopkins, S. LePape, T. Ma, P. K. Patel, B. A. Remington, H. F. Robey, J. D. Salmonson, and J. L. Kline, Phys. Rev. Lett. **112**, 055001 (2014)
[19] V. N. Goncharov, J. P. Knauer, P. M. McKenty, P. B. Radha , T. C. Sangster , S. Skupsky , R. Betti , R. L. McCrory , and D. D. Meyerhofer, Phys. Plasmas **10**, 1906 (2003)
[20] K. Anderson, R. Betti, Phys. Plasmas **10**, 4448 (2003)
[21] V. A. Smalyuk, V. N. Goncharov, K. S. Anderson R. Betti, R. S. Craxton, J. A. Delettrez, D. D. Meyerhofer, S. P. Regan and T. C. Sangster, Phys. Plasmas **14**,032702 (2007)
[22] R. Betti, K. Anderson, J. P. Knauer, T. J. B. Collins, R. L. McCrory, P. W. McKenty and S. Skupsky, Phys. Plasmas **12**, 042703 (2005)
[23] N. Metzler, A. L. Velikovich, and J. H. Gardner, Phys. Plasmas **6**, 3283 (1999)
[24] D. S. Clark, J. L. Milovich, D. E. Hinkel, J. D. Salmonson, J. L. Peterson, L. F. Berzak Hopkins, D. C. Eder, S. W. Haan, O. S. Jones, M. M. Marinak, H. F. Robey, V. A. Smalyuk and C. R. Weber, Phys. Plasmas, **21**, 112705 (2014)
[25] J. L. Peterson, L. F. Berzak Hopkins, O. S. Jones and D. S. Clark, Phys. Rev. E, 91, 031101(R) (2015)
[26] V. A. Smalyuk, *et al*., under review Phys. Plasmas.
[27] J. L. Peterson, D. S. Clark, L. P. Masse and L. J. Suter, Phys. Plasmas **21**, 092710 (2014)
[28] Y. Aglitskiy, A. L. Velikovich, M. Karasik, V. Serlin, C. J. Pawley, A. J. Schmitt, S. P. Obenschain, A. N. Mostovych, J. H. Gardner, and N. Metzler , Phys. Plasmas **9**, 2264 (2002)
[29] O. V. Gotchev, V. N. Goncharov, J. P. Knauer, T. R. Boehly, T. J.B. Collins, R. Epstein, P. A. Jaanimagi, and D. D. Meyerhofer, Phys. Rev. Lett. **96**, 115005 (2006)
[30] E. Loomis, D. Braun, S. H. Batha, and O. L. Landen, Phys. Plasmas **19** 122703 (2012)
[31] A. Casner, L. Masse, B. Delorme, D. Martinez, G. Huser, D. Galmiche, S. Liberatore, I. Igumenshchev, M. Olazabal-Loumé, Ph. Nicolaï, J. Breil, D. T. Michel, D. Froula, W. Seka, G. Riazuelo, S. Fujioka, A. Sunahara, M. Grech, C. Chicanne, M. Theobald, N. Borisenko, A. Orekhov, V. T. Tikhonchuk, B. Remington, V. N. Goncharov, and V. A. Smalyuk, Phys. Plasmas **21**, 122702 (2014)
[32] J. L Peterson, D. T. Casey, O. A. Hurricane, K. S. Raman, H. F. Robey, and V. A. Smalyuk, Phys. Plasmas **22**, 056309 (2015)
[33] M. M. Marinak, G. D. Kerbel, N. A. Gentile, O. Jones, D. Munro, S. Pollaine, T. R. Dittrich and S. W. Haan, Phys. Plasmas **8**, 2275 (2001)
[34] J. L. Milovich et al., submitted to Phys. Plasmas
[35] L. M. Barker, R. E. Hollenbach, J. Appl. Phys. **43** 4669 (1972); L. M. Barker, R. E. Hollenbach, J. Appl. Phys. **45** 3692 (1974)
[36] K. L. Baker, H. F. Robey, J. L. Milovich, O. S. Jones, V. A. Smalyuk, D. T. Casey, A. G. MacPhee, A. Pak, P. M. Celliers, D. S. Clark, O. L. Landen, J. L. Peterson, L. F. Berzak-Hopkins, C. R. Weber, S. W. Haan, T. D. Döppner, S. Dixit, E. Giraldez, A. V. Hamza, K. S. Jancaitis, J. J. Kroll, K. N. Lafortune, B. J. MacGowan, J. D. Moody, A. Nikroo and C. C. Widmayer, Phys. Plasmas **22**, 052702 (2015)
[37] V. A. Smalyuk, D. T. Casey, D. S. Clark, M. J. Edwards, S. W. Haan, A. Hamza, D. E. Hoover, W. W. Hsing, O. Hurricane, J. D. Kilkenny, J. Kroll, O. L. Landen, A. Moore, A. Nikroo, L. Peterson, K. Raman, B. A. Remington, H. F. Robey, S. V. Weber and K. Widmann, Phys. Rev. Lett. **112** 185003 (2014); K. S. Raman, V. A. Smalyuk, D. T. Casey, S. W. Haan, D. E. Hoover, O. A. Hurricane, J. J. Kroll, A. Nikroo, J. L. Peterson, B. A. Remington, H. F. Robey, D. S. Clark, B. A. Hammel, O. L. Landen, M. M. Marinak, D. H. Munro, K. J. Peterson and J. Salmonson, Phys. Plasmas **21**, 072710 (2014)
[38] O. L. Landen, J. Edwards, S. W. Haan, H. F. Robey, J. Milovich, B. K. Spears, S. V. Weber, D. S. Clark, J. D. Lindl, B. J. MacGowan, E. I. Moses, J. Atherton, P. A. Amendt, T. R. Boehly, D. K. Bradley, D. G. Braun, D. A. Callahan, P. M. Celliers, G. W.

Collins, E. L. Dewald, L. Divol, J. A. Frenje, S. H. Glenzer, A. Hamza, B. A. Hammel, D. G. Hicks, N. Hoffman, N. Izumi, O. S. Jones, J. D. Kilkenny, R. K. Kirkwood, J. L. Kline, G. A. Kyrala, M. M. Marinak, N. Meezan, D. D. Meyerhofer, P. Michel, D. H. Munro, R. E. Olson, A. Nikroo, S. P. Regan, L. J. Suter, C. A. Thomas and D. C. Wilson, Phys. Plasmas **18**, 051002 (2011)
[39] M. A. Barrios, D. G. Hicks, T. R. Boehly, D. E. Fratanduono, J. H. Eggert, P. M. Celliers, G. W. Collins and D. D. Meyerhofer, Phys. Plasmas **17**, 056307 (2010)